Int J Adv Manuf Technol (2017) 91:3427–3435
DOI 10.1007/s00170-016-9974-5

ORIGINAL ARTICLE

Role of insert material on process loads during FSW

Saurabh Dixit[1] · **Madhu H. C.**[2] · **S. V. Kailas**[2] · **K. Chattopadhyay**[1]

Received: 27 January 2016 / Accepted: 26 December 2016 / Published online: 23 January 2017

Abstract In FSW, insert materials are often used to both control the loading conditions as well as to trace the nature of materials flow. This current study aims at understanding the role played by inserts materials by using two different materials, copper and tin as inserts. The copper and tin have higher and lower melting points respectively as compared to aluminum. The metal strips are sandwiched between aluminum plates and friction stir welded at two different rotational speeds. The process loads and torque were recorded during the welding and compared with that obtained for normal butt-welding of aluminum sheets. In the case of copper insert, copper gets distributed in the matrix and it is possible to trace the flow of copper inside the aluminum. In the case of tin, it melts during the welding. The molten tin is squeezed out of faying surface and coats tool shoulder. This lowers the friction and which in turn lowers the torque (55%) and the consequent heat generation. The resultant reduction of temperature in the weld leads to higher tangential and normal loads. Compared to the case without insert, the normal loads for FSW processing with tin insert were higher by 2.2 times and tangential loads were higher by 5.5 times.

Keywords FSW · Melting · Process loads · Inserts

✉ Saurabh Dixit
saurabhdixit11@gmail.com

[1] Department of Materials Engineering, Indian Institute of Science, Bangalore 560012, India

[2] Department of Mechanical Engineering, Indian Institute of Science, Bangalore 560012, India

1 Introduction

Friction Stir Welding (FSW) is one of the attractive solid state welding techniques suitable for welding light metals and alloys such as aluminum and magnesium alloys [1]. This is often preferred for precipitation hardened aluminum alloys that were not recommended for welding with conventional fusion welding techniques. The primary drawback of fusion welding techniques is the adverse microstructural changes that occur during melting and resolidification caused by wide temperature range of solidification and resulting residual stress and distortion of the welds [2, 3]. Stress corrosion cracking of 7xxx series alloys was also a serious issue during fusion welding. All these material can easily be welded using FSW technique with much higher weld efficiencies, lower residual stresses and even compressive residual stresses and lower distortion [4]. The feasibility of joining steels using FSW technique was demonstrated by Thomas et al. [5] in 1999. In 1998 Murr et al. [6] pioneered dissimilar welding by this technique and demonstrated joining of sheets of Al 6061-T6 to copper by FSW. Since then a significant amount of work has been carried out on dissimilar metal welding using FSW. Joining of aluminum to copper [7, 8], aluminum alloys to titanium and its alloys [9, 10], aluminum to magnesium-based alloys [11], magnesium to titanium alloys [12], and even aluminum to steel [13, 14], have been carried out by FSW.

The incipient melting, during FSW, of certain phases or coatings such as zinc coating are of serious concern since these melted phases can form undesirable intermetallics. Cracks and voids were also noticed in such cases [15, 16]. The incipient melting was also reported during welding of certain aluminum alloys [17, 18].

To enhanced the properties of weld joint, several researchers have sandwiched a strip or foil of third material between two plates [19–21]. Lee et al. [22] coated the weld

surface with Ni before carrying out lap joint of steel with a Ni-Cu alloy. Inada et al. [19] filled copper powder in between the gap of the aluminum plate during butt welding. Shiri et al. [21] studied the effect of copper, zinc, and nickel foils placed along the longitudinal side of pure Al workpieces during welding and have shown that the strength of the weld joint can be improved by these strips. Inserts are also used to understand material flow in FSW process. [23–25]. Colligan, K [25] used the steel balls to trace the material flow.

The insert materials also act as flow markers. Copper, aluminum alloys, gold foil [26], zinc [21], lead [27] are some of the materials used for this purpose. Doude et al. [27] have used lead as a marker material that melted and provided a continuous trace of the metal flow during the FSW process. Schneider et al. [28, 29], on the other hand, used high melting tungsten wire as a marker. Although numerous studies have been carried out using marker and insert materials, none of the works have studied the effect of these inserts on the processing loads and temperature. Any change in these can have a significant effect on the flow of materials, thereby, affecting the interpretation of the results. Hence there is a need to understand the behavior of inserts, particularly from the perspective of their effect on processing parameters like the loads and temperatures during the FSW operation.

In friction stir welding, materials move around the tool and gets extruded from leading side of the tool to the trailing side. Two forces, a tangential force (x-axis force), perpendicular to the tool axis, and a normal force (Z-axis force), normal to the tool axis, along with a torque are required to carry out the welding. The X-axis force is a force required to push the tool in the forward direction along the weld line, while the Z-axis force is a normal load required to plunge the tool to a given depth. This study aims to understand the effect of inserts on these forces during FSW process.

Thin strips of two different materials, tin and copper were selected for this study. The melting temperate of tin is lower than FSW temperature while melting temperature of copper is well above the process temperature. A comparative study of the process loads (X, Z- axis and Torque) during the FSW for different processing conditions are also presented.

2 Experiment

To study the effect of insert material at the faying surface of weld during the FSW processes, commercially pure aluminum plates of 6 mm thick and 70 mm wide and 200 mm long were butt-welded. The faying surface of aluminum sheets were milled and ground using a belt grinder to achieve uniform surface roughness. Figure 1a & b shows the schematic of the

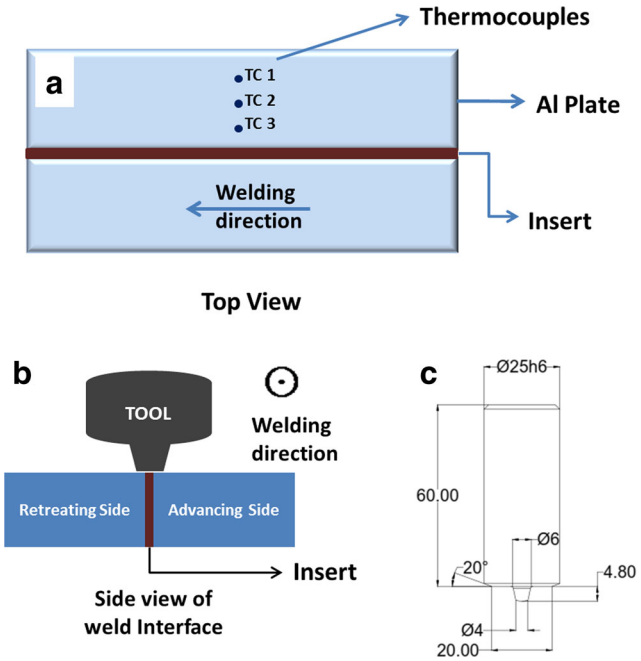

Fig. 1 Schematics of the insert and thermocouples location in the weld (a) top view (b) side view (c) schematic of FSW tool

geometry of the work piece used in the current FSW process. Tin (99.9% pure) and copper (99.9% pure) of 0.18 mm thickness were used as inserts.

A plain conical tool made of tool steel was used for the study. The shoulder diameter of the tool was 20 mm and the pin height was 4.8 mm; the diameter of the pin varied from 6 mm at the top to 4 mm at the bottom (Fig. 1(c)). The FSW experiments were carried out at rotational speeds of 750 and 1050 rpm for a length of 160 mm. Tool travel speed was 60 mm/min. A plunge depth of 4.9 mm and tool tilt angle of 2^{o} were used for all the experiments. An initial hold for ten seconds for the rotating tool was given after plunging of the tool and before the start of the weld. The 'K' type thermocouples along with a data logger were used to measure the temperature at a rate of 10 Hz. Thermocouples were fixed at a depth of 3 mm from the top surface of the plate and at a distance of 15 mm, 25 and 35 mm, on the retreating side as shown in Fig. 1(a).

All the FSW experiments were carried out using a machine designed in house and built by ETA Technologies Pvt. Ltd., Bangalore, India. An AC servo motor of Rexroth make is used to rotate the tool. The aluminum plates are clamped vertically. The spindle assembly is controlled by a servo hydraulic system with an accuracy of 1 μm (Z- axis), with and a load capacity of 100kN in the Z direction. The load cells used can measure forces up to 70 kN and 100 kN respectively in X-axis and Z-axis directions. All the load cells can acquire

data with a frequency of 20 Hz. Controller modules from National Instruments (NI cRio-9012 and 9102) are used to control the machine. The machine is controlled by a PC system using LabVIEW software (National Instruments make).

Samples for microstructure analysis were cut from the weldment in a direction perpendicular to the welding track. Samples were mechanically ground using SiC papers from 400 to 3000 grit and subsequently polished on velvet cloth impregnated with alumina slurry of particle size below 1 μm. SEM (FEI make), equipped with EDS detector (EDAX make), was used for microstructural analysis of the samples.

3 Results

Experiments were carried out under three different interface conditions; a) Insert of pure Sn, b) Insert of pure copper and c) tool without any insert. The first set of experiments were performed at 750 rpm with 60 mm/min of tool travel velocity and a tool tilt of two degrees. For the second set of experiments, tool rotational speed was increased to 1050 rpm. The loads and temperatures were recorded for all the experiments.

3.1 Set 1: tool rotational speed of 750 rpm

Figure 2 shows Z-axis load (normal load) during the first set of experiments. The transition points from plunging operation to initial heating and initial heating to tool travel are marked with vertical lines in the figure. The Z-axis load during the steady state tool travel was much higher with tin insert, as compared to the welds with Cu insert or no insert. The lowest load was recorded for welds without any inserts at the faying surface of the butt weld. The average steady state Z-axis load was around 14.7 KN and 6.5 KN for tin insert welds and without any insert welds, respectively.

Figure 3 shows X-axis load (traverse load) for the same set of experiments. Similar to Z-axis loads, X-axis load was much higher for tin insert welds, which was ~2.2 KN. For weld without insert, X-axis weld was ~0.4 kN and in the case of the copper, the load was marginally higher than without insert weld.

Figure 4 shows spindle torque for all the three conditions. The steady state torque was least for welds with tin insert, which was around 16.2 Nm. The highest torque (29.2 Nm) was obtained for welds without any inserts. It can be seen that the torque reaches its maximum value when tool shoulder initially contacts the workpiece. Drop in torque was observed after initial shoulder contact in welds without insert and Cu insert, whereas no such drop is observed welds with tin insert.

The peak temperature recorded by the individual thermocouple is plotted in Fig. 5(a). The peak temperatures were extrapolated to the boundary of the nugget zone, which is at 10 mm from weld central line. The temperature is assumed to be constant within the weld nugget. It is to be noted that the temperature within the nugget zone is difficult to determine experimentally due to large plastic strains that damage the thermocouples.

Temperatures during all the experiments of Set 2 were recorded and the peak temperatures of each thermocouple were plotted in Fig. 5(b). For the second set of experiments, the nugget temperature was maximum for welds without insert (457 °C, 0.78 Tm), and minimum for welds with tin insert (252 °C, 0.5Tm). The temperature profiles of the weld done with copper insert and without any insert were similar. The temperature recorded in the weld without insert is consistent

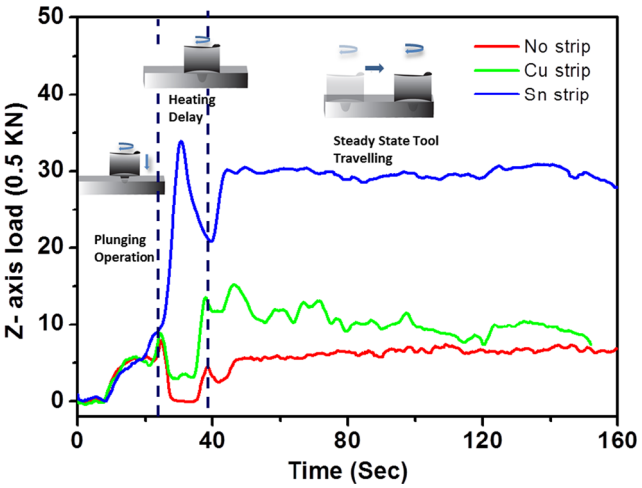

Fig. 2 Variation of Z-axis loads during FSW of Al plates with different inserts at a tool rotation speed of 750 rpm. The loads were unexpectedly high for Sn insert weld

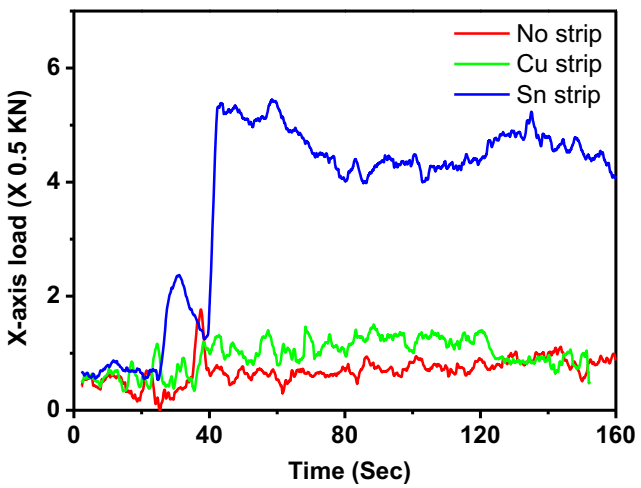

Fig. 3 Variation of X-axis loads during FSW of Al plates with different insert at a tool rotation speed of 750 rpm. The loads were unexpectedly higher when Sn insert weld

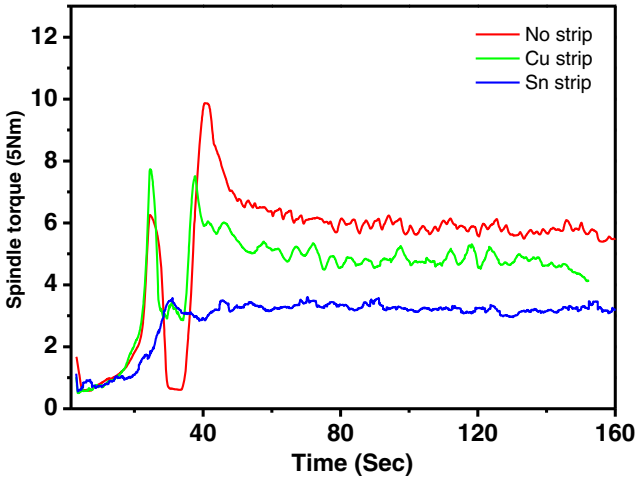

Fig. 4 Variation of spindle torque during FSW of Al plates with different insert markers. The torque was lower during the steady state tool travel when Sn insert weld

with results reported by Shinoda et al. [30]. Shinoda et al. have reported a peak temperature of the nugget zone during the FSW butt-welding of the commercially pure aluminum sheet to be 450 °C (0.77 Tm) at 1100 rpm with a tool travel speed of 150 mm/min. Hwang et al. [31] have used 6061 aluminum sheets for the experiment and showed that the peak temperature to be around 407 °C (0.72 Tm). Tang et al. [32] and others [33] showed that the peak temperature of FSW welding of aluminum 6061-T6 was around 425 °C to 477 °C. (0.75–0.8 Tm) Chao et al. [34] had measured the temperature of the nugget zone during the FSW welding of 2195-T8 aluminum alloy and reported the peak temperature of the weld nugget to be around 420 °C(0.74 Tm).

Figure 6 shows low magnification SEM micrograph of nugget during welding with copper insert. The microstructure indicates the fragmentation of copper strip into small particles on advancing side (AS) of the nugget. In contrast, few larger particles can be seen on the retreating side (RS). Figure 7(a) shows SEM micrograph of the weld that contains tin insert. Tin particles were surprisingly missing in this micrograph. A collage of backscattered SEM micrograph is shown in Fig. 7. The inset image (Fig. 7(b)) shows central region of nugget zone at higher magnification. Fine bright particles seen are identified as tin particles by using EDS point analysis (Fig. 7(d)). Figure 7(c) shows the higher magnification SEM micrograph of the bottom section of the nugget zone with a fine crack and trace amount of tin.

3.2 Set 2: rotational speed of 1050 rpm

In the next set of experiments, the rotational speed of the FSW tool was increased to 1050 rpm while other

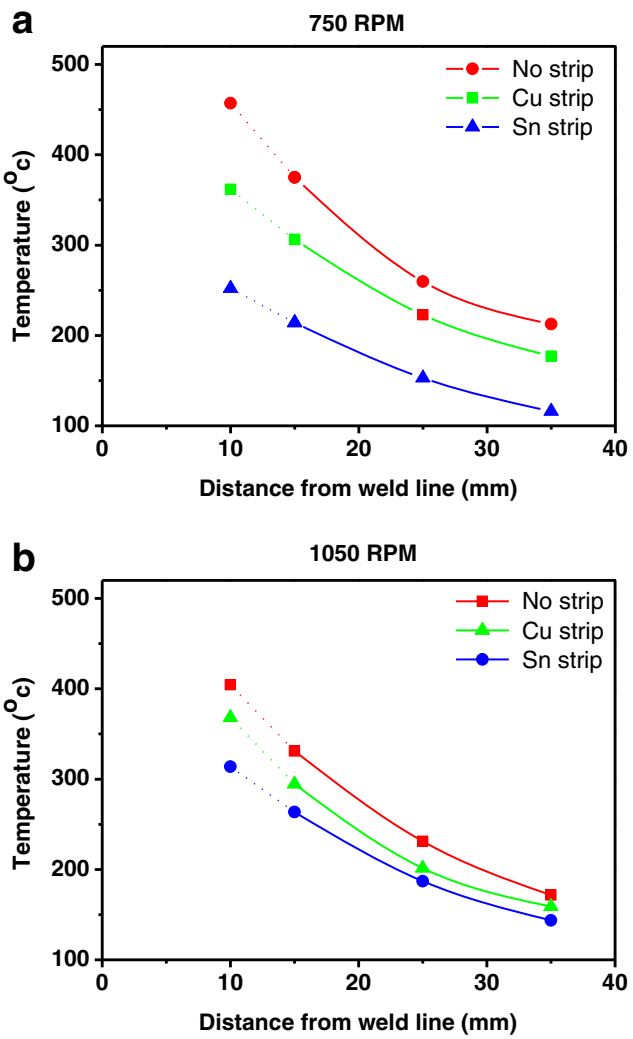

Fig. 5 Temperature profile during the FSW of Al at two different tool rotation speeds (a) 750 (b) 1050 rpm. Temperature of nugget zone was lowest for the Sn insert weld

welding conditions were kept identical to understand the effect of rpm on process loads and peak temperatures in the presence of different insert materials. Figures 8(a) and (b) show Z axis load of FSW weld carried out at 1050 rpm using copper and tin as an insert material respectively. The Z-axis loads were also compared for welds carried out at 750 rpm. It can be seen from Fig. 8(a) that the Z-axis load during steady state was similar for both the tool rpms in the case of copper insert. However, in the case of tin, there is a significant difference in steady state Z-axis loads for 750 and 1050 rpm welds. As can be seen, 750 rpm weld experiences higher load compared to 1050 rpm.

X-axis loads during FSW welding at 1050 rpm and 750 rpm with the copper insert are plotted in Fig. 9(a), and

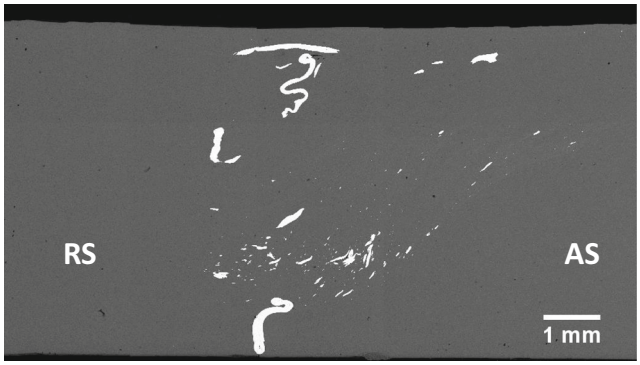

Fig. 6 Backscattered SEM macrograph of weld nugget with Cu insert. Cu was distributed in the weld nugget

that with tin, inserts are plotted in Fig. 9(b). As can be seen from the X-axis load data, the loads were same for both conditions for copper insert welds. However, in the case of tin insert, the loads during the steady state tool travel were lower for 1050 rpm. X-axis loads for both the rpm conditions were higher for the case of tin insert.

Figure 10(a) and (b) shows spindle torque recorded during the experiments. Figure 10(a) shows the spindle torque for welds with copper insert carried out s at 750 and 1050 rpms. Figure 10(b) shows the torque for welds with tin insert under the identical welding conditions. In the case of tin insert, torque was lower than that of the copper insert. Further, for this case, the torque does not vary significantly with change in rotational speeds. In contrast, torque during weld reduces with increase in rotational speed for copper insert.

4 Discussion

The welds with copper inserts and without insert show Z axis loads which are characteristic to FSW (Figs. 2 and 8(a) respectively). The Z-axis load increases during the tool plunging operation and reaches a maximum value as the tool initially plunges. This is consistent with the results of Zimmer et al., who have shown that Z-axis load increases during tool plunging operation [35]. Further, the load reaches a lower value during the heating period. Atharifar et al. have shown similar trend during FSW welding of aluminum 6061 [36]. They have shown that X-axis force is mainly governed by tool travel speed while torque is governed by tool RPM. These authors have also validated their results using a numerical model. A similar trend in FSW welding of aluminum 2024 was established by Su et al. [37]. These investigators have shown that a faster rotation speeds lead to lower torque while tool travel speed has negligible influence on the torque.

However, in the case of tin insert welds, Z-axis load exhibits an abnormal behavior. The steady sate Z-axis load, in this case, was significantly high compared to that observed for weld with copper insert and welds without insert. No plateau was observed during the initial heating by the tool. The load decreases at relatively low rate after completion of plunging. Tin being a softer material, the loads were expected to be lower, but actual observation indicates an increase. The Z-axis load was about 5 times higher in the case of welds with tin insert compared to the welds without inserts. A similar behavior was also observed for X-axis load (Figs. 3 and 10),

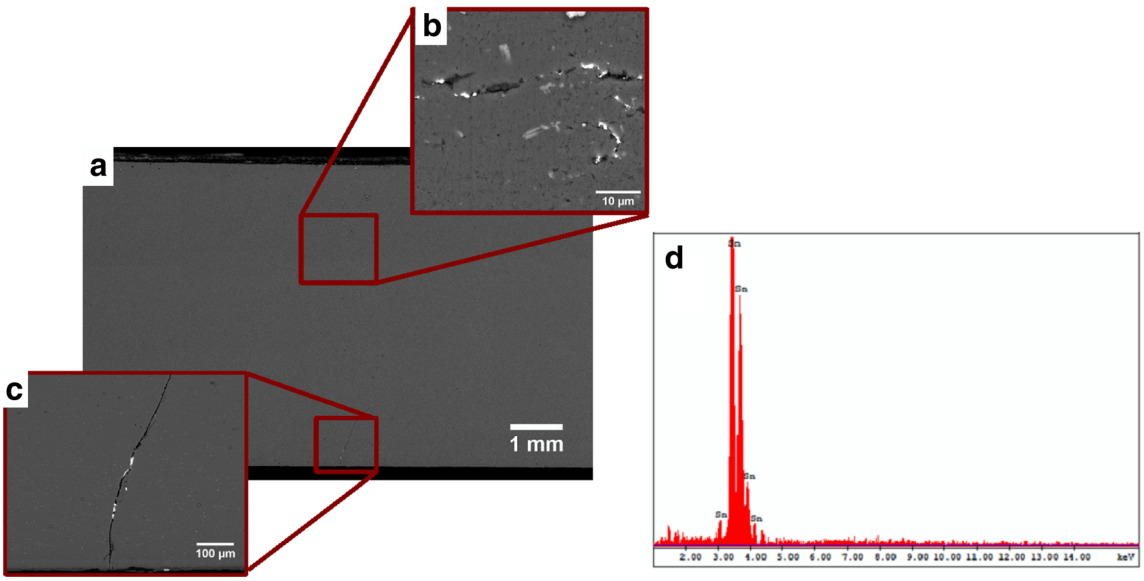

Fig. 7 Backscattered SEM macrograph of weld nugget with Sn insert (a) low magnification image (b) and (c) at higher magnification (d) EDS spectra of bright particles

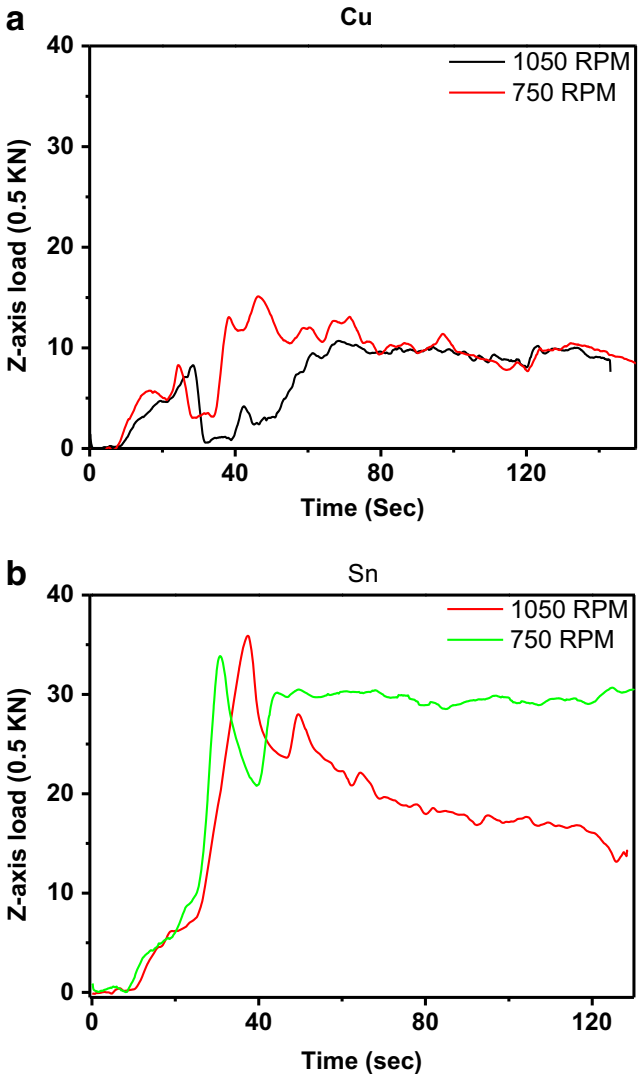

Fig. 8 Effect of tool rotation speed on Z-axis loads during FSW of Al with different inserts (a) Cu insert (b) Sn insert

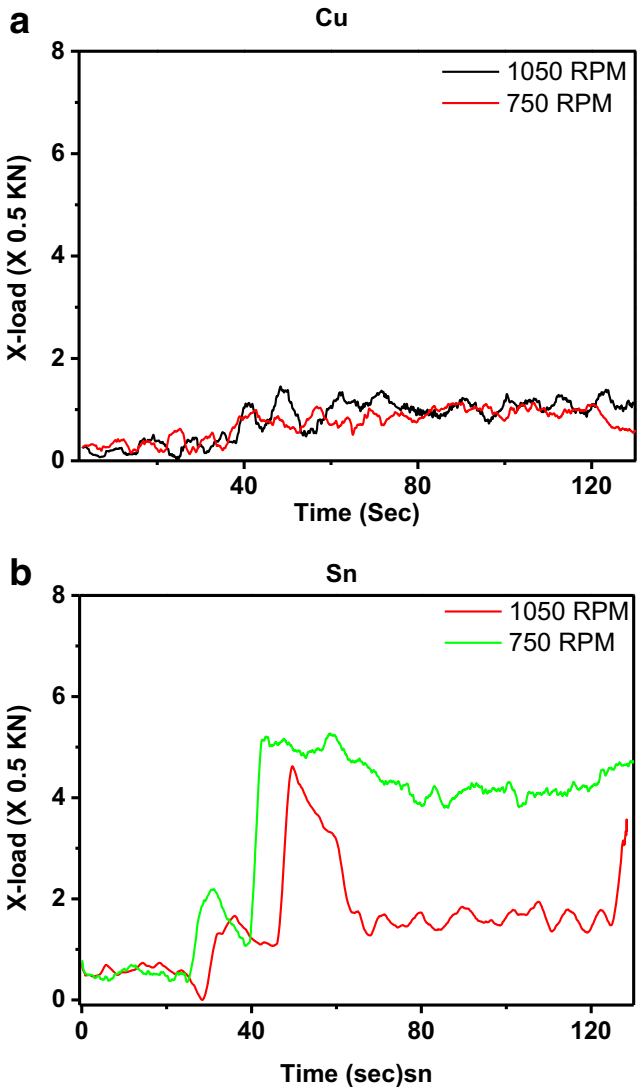

Fig. 9 Effect of tool rotation speed on X-axis loads during FSW of Al with different inserts (a) Cu insert (b) Sn insert

where the peak load, during tin insert welds were found to be around 5.5 times higher than the loads observed during welding with copper insert.

4.1 Melting of tin during FSW

The temperate in the nugget zone exceeds the melting temperature of the tin (232 °C) during FSW (Fig. 5). This leads to melting of tin during welding. Due to heat transfer tin melts well ahead of the tool. This molten layer of tin, due to capillary action, is held between the aluminum plates. The molten tin coats shoulder of the tool and hence reduces friction between the tool and the workpiece (Fig. 11(c)). As the friction reduces, the torque for a given speed, drops. The average torque is reduced by s ~ 13.5 Nm during welding with tin insert compared to the welds without inserts.

The friction between the tool and workpiece provides the maximum share of the total heat generated during the process [38, 39]. The heat generation can be calculated by the formula given by Frigaard et al. [38]

$$q = \frac{3}{4}\pi^2 \mu p N R^3$$

Where q is total heat input per unit time, μ the coefficient of friction, p contact pressure, N number of rotation per unit time, and R is the shoulder diameter.

In the equation, the quantity μ, the coefficient of friction reduces due the presence of tin coating between the tool and work piece. Hence, the total heat input would also reduce. Consequently, the temperature of the nugget zone drops as compared to other welds (Fig. 5). The lower processing

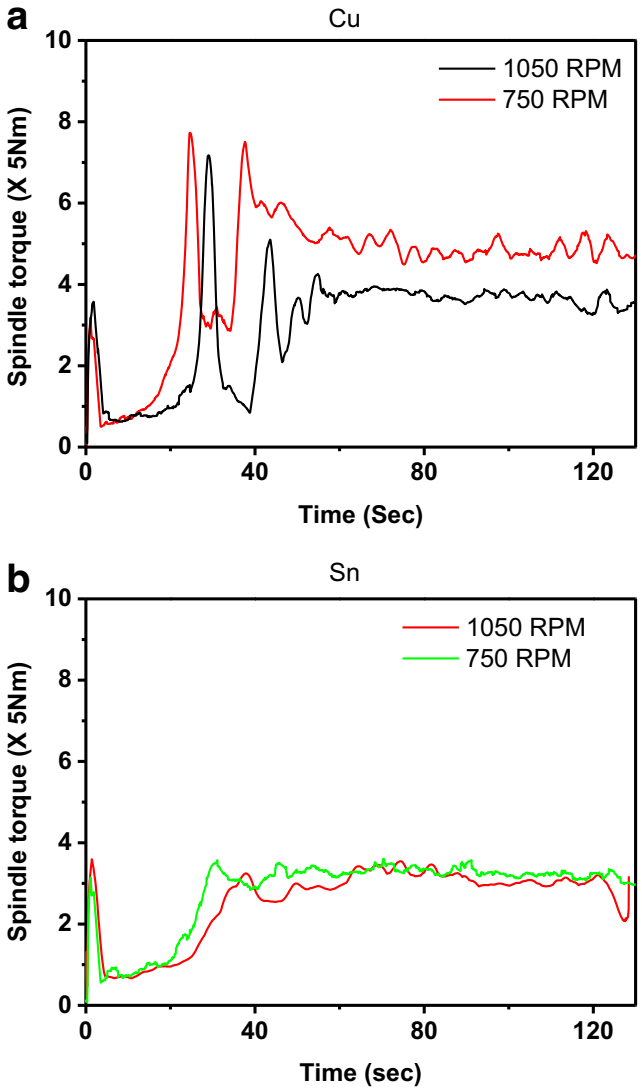

Fig. 10 Effect of tool rotation speed on spindle torque during FSW of Al with different inserts (a) Cu insert (b) Sn insert

temperature leads to change in flow behavior of the plasticized material around the tool pin.

Figure 11(a) shows the top surface of tin insert weld done at 750 rpm. EDS analysis of the image confirms that the phase with bright contrast is tin while the one with dark contrast is aluminum. The tin was coated mostly on retreating side, as the material transfers from advancing side to retreating side. Inset in Fig. 11(b) shows a higher magnification image of the top surface of the weld nugget. The serration mark due to the tool advancement is clearly visible. The separation between two marks was measured to be around 0.08 mm, which is equal to the APR (advancement per revolution) of the tool. APR is an important quantity in FSW. Sutton et al. [40], as well others [18, 41], have established that APR is directly related to the instantaneously deforming volume size, as the tool sweeps this volume of material in each revolution [41].

The copper particles were clearly visible in the nugget as seen in Fig. 6, whereas tin particles were absent in the nugget (Fig. 7(a)). As the tool moves, the molten tin is squeezed out due to compressive forces ahead of the tool. Traces of the tin were found at the nugget (Fig. 7(b)).

4.2 Effect of the melting of tin on the process loads

The presence of even a small amount of tin or any other material, whose melting point is lower than the FSW process temperature, especially when it is immiscible, can change the FSW process loads significantly. The melting of such material leads to the reduction in frictional heat, which is an essential part of FSW. This heat softens the material; hence the material flows around the tool with ease. Now when the quantity of heat input was less, larger forces were required to consolidate the material beneath the tool shoulder and for the tool to move forward. As shown in Figs. 2 and 3 respectively, Z-axis and X-axis loads for tin insert case were enormously high. The increase in rotational speed has a significant influence on Z and X- axis loads of FSW welds for welding with tin insert. However, change in rotational speed did not affect these loads during the steady-state tool travel for welds with copper insert. We note that there was no significant change in spindle torque in case of the tin insert for different rotational speed while in the case of copper insert the torque reduces. Yan et al. [17] experimentally showed that the torque reduces rapidly when rotational speed was increased from 150 to 600 rpm and afterwards rate of change in torque with an increase in rotational speed was low for aluminum 2024 alloy. Arora et al. [42] showed numerically that torque required for FSW decreases with increase in tool rotation speed. These authors suggested that it is easy for material to stir at a higher temperature and higher strain rate. As we can see from Fig. 5, there was an increase in the temperature when rotational speed was increased to 1050 rpm for the case of the tin insert; however, the temperature was still lower if we compare it with the cases of copper insert or without any insert. Hence, Z and X- axis loads for welding at 1050 rpm with tin insert reduce due to the increase in temperature, which leads to the more softening of the material.

Drastic reduction in torque was observed when the tin insert was used as marker material as incipient melting of tin occurs. We note that tin is insoluble in aluminum. However, this does not mean that any marker material with a lower melting point than the aluminum will show similar result. The work carried out by Shiri et al. [21] using zinc as a marker material in the welding of aluminum resulted in a weld of good quality. The micrograph shown in the study did not show any

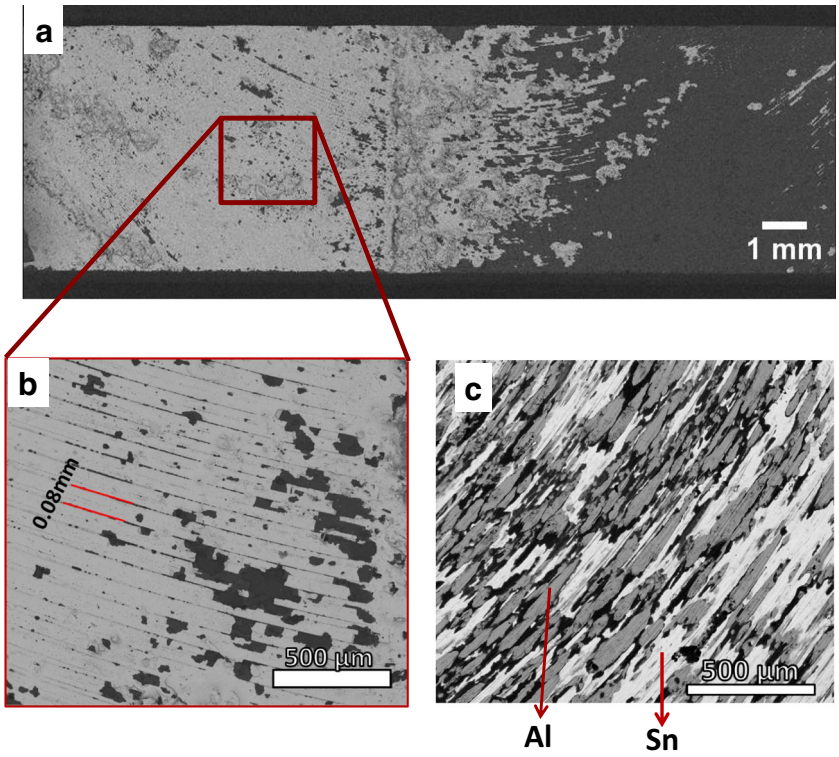

Fig. 11 (a) SEM-BSE image of top surface of weld with Sn insert. Layer of tin with white contrast is clearly visible in the image (b). Image at higher magnification. The spacing between two tool marks is equal to the APR of the welding. (C) SEM-BSE image of the tool shoulder showing Sn and Al coating

micro cracks. This suggests that the solubility of insert material also plays a role towards the forces generated during the welding process.

5 Conclusion

In the present study, it has been shown that the presence of insert materials that has lower melting temperature than the FSW processing temperature, will melt. This leads to a higher processing loads and lowers the processing temperature. However, the torque is also reduced in such cases. The increase in rotational speed will lead to a reduction in process load due to increasing in process temperature, while it has little effect on torque. The melted insert material forced out due to the compressive forces that develop during the process and coats the top surface of the weld nugget as well as the tool shoulder. This coating of insert material on the tool shoulder leads to the reduction in spindle torque and frictional heat. This analogy can be extended to where incipient melting of any phase is expected. The melting of any phase can be identified by studying the torque. The melting of a phase leads to a reduction in torque, followed by a decrease in process temperature.

A fine crack was observed for the weld with tin insert. This crack would lead to degradation of the quality of the weld. Hence, the relatively low melting point insoluble material is neither a suitable candidate to sandwich between two plates nor as a marker material to understand the material flow unless the process parameters are re-optimized. However, in certain cases, such inserts may be useful where low operating torque and processing temperature is desired.

Acknowledgements The authors would like to acknowledge the microscopy facility available at Advanced Facility for Microscopy and Microanalysis (AFMM) centre. Partial support from a grant from Naval Research Board, Government of India to one of the authors (KC) is gratefully acknowledged.

References

1. Mishra RS, Ma ZY (2005) Friction stir welding and processing. Mater Sci Eng R Rep 50:1–78. doi:10.1016/j.mser.2005.07.001
2. Barnes T, Pashby I (2000) Joining techniques for aluminium spaceframes used in automobiles. J Mater Process Technol 99: 62–71. doi:10.1016/S0924-0136(99)00367-2
3. Zhao H, White DR, DebRoy T (1999) Current issues and problems in laser welding of automotive aluminium alloys. Int Mater Rev 44: 238–266. doi:10.1179/095066099101528298
4. Nadammal N, Kailas SV, Suwas S (2015) A bottom-up approach for optimization of friction stir processing parameters; a study on aluminium 2024-T3 alloy. Mater Des 65:127–138. doi:10.1016/j.matdes.2014.09.005
5. Thomas WM, Threadgill PL, Nicholas ED (1999) Feasibility of friction stir welding steel. Sci Technol Weld Join 4:365–372. doi:10.1179/136217199101538012
6. Murr LE, Li Y, Flores RD et al (1998) Intercalation vortices and related microstructural features in the friction-stir welding of

dissimilar metals. Mater Res Innov 2:150–163. doi:10.1007/s100190050078
7. Al-Roubaiy AO, Nabat SM, Batako ADL (2014) Experimental and theoretical analysis of friction stir welding of Al–Cu joints. Int J Adv Manuf Technol 71:1631–1642. doi:10.1007/s00170-013-5563-z
8. Carlone P, Astarita A, Palazzo GS et al (2015) Microstructural aspects in Al–Cu dissimilar joining by FSW. Int J Adv Manuf Technol 79:1109–1116. doi:10.1007/s00170-015-6874-z
9. Chen YC, Nakata K (2009) Microstructural characterization and mechanical properties in friction stir welding of aluminum and titanium dissimilar alloys. Mater Des 30:469–474. doi:10.1016/j.matdes.2008.06.008
10. Dressler U, Biallas G, Alfaro Mercado U (2009) Friction stir welding of titanium alloy TiAl6V4 to aluminium alloy AA2024-T3. Mater Sci Eng A 526:113–117. doi:10.1016/j.msea.2009.07.006
11. Sheikh-Ahmad JY, Ozturk F, Jarrar F, Evis Z (2016) Thermal history and microstructure during friction stir welding of Al–Mg alloy. Int J Adv Manuf Technol. doi:10.1007/s00170-015-8239-z
12. Aonuma M, Nakata K (2012) Dissimilar metal joining of ZK60 magnesium alloy and titanium by friction stir welding. Mater Sci Eng B 177:543–548. doi:10.1016/j.mseb.2011.12.031
13. Uzun H, Dalle Donne C, Argagnotto A et al (2005) Friction stir welding of dissimilar Al 6013-T4 to X5CrNi18-10 stainless steel. Mater Des 26:41–46. doi:10.1016/j.matdes.2004.04.002
14. Schneider J, Radzilowski R (2014) Welding of very dissimilar materials (Fe-Al). JOM 66:2123–2129. doi:10.1007/s11837-014-1134-5
15. Kumar N, Yuan W, Mishra RS (2015) Friction stir welding of dissimilar alloys and materials. Butterworth-Heinemann, UK
16. Robson JD, Cui S, Chen ZW (2010) Incipient melting during friction stir processing of AZ91 magnesium castings. Mater Sci Eng A 527:7299–7304. doi:10.1016/j.msea.2010.07.093
17. Yan J, Sutton MA, Reynolds AP (2005) Process–structure–property relationships for nugget and heat affected zone regions of AA2524–T351 friction stir welds. Sci Technol Weld Join 10:725–736. doi:10.1179/174329305X68778
18. Long T, Tang W, Reynolds AP (2007) Process response parameter relationships in aluminium alloy friction stir welds. Sci Technol Weld Join 12:311–317. doi:10.1179/174329307X197566
19. Inada K, Fujii H, Ji YS et al (2010) Effect of gap on FSW joint formation and development of friction powder processing. Sci Technol Weld Join 15:131–136. doi:10.1179/136217109X12568132624244
20. Chang W-S, Rajesh SR, Chun C-K, Kim H-J (2011) Microstructure and mechanical properties of hybrid laser-friction stir welding between AA6061-T6 Al alloy and AZ31 Mg alloy. J Mater Sci Technol 27:199–204. doi:10.1016/S1005-0302(11)60049-2
21. Shiri SG, Sarani A, Hosseini SRE, Roudini G (2013) Diffusion in FSW joints by inserting the metallic foils. J Mater Sci Technol 29:1091–1095. doi:10.1016/j.jmst.2013.07.003
22. Lee R-T, Liu C-T, Chiou Y-C, Chen H-L (2013) Effect of nickel coating on the shear strength of FSW lap joint between Ni–Cu alloy and steel. J Mater Process Technol 213:69–74. doi:10.1016/j.jmatprotec.2012.07.014
23. Seidel TU, Reynolds AP (2001) Visualization of the material flow in AA2195 friction-stir welds using a marker insert technique. Metall Mater Trans A 32:2879–2884. doi:10.1007/s11661-001-1038-1
24. Schmidt HNB, Dickerson TL, Hattel JH (2006) Material flow in butt friction stir welds in AA2024-T3. Acta Mater 54:1199–1209. doi:10.1016/j.actamat.2005.10.052
25. Colligan K (1999) Material flow behavior during friction welding of aluminum. Weld J 75:229s–237s
26. Kang SH, Han HN, Oh KH et al (2009) Investigation of the material flow and texture evolution in friction-stir welded aluminum alloy. Met Mater Int 15:1027–1031. doi:10.1007/s12540-009-1027-2
27. Doude HR, Schneider JA, Nunes AC (2014) Influence of the tool shoulder contact conditions on the material flow during friction stir welding. Metall Mater Trans A 45:4411–4422. doi:10.1007/s11661-014-2384-0
28. J.A. Schneider, A.C. Nunes, Jr (2006) Influence of processing parameters on the flow path in friction stir welding. ntrs.nasa.gov
29. Schneider J, Beshears R, Nunes AC (2006) Interfacial sticking and slipping in the friction stir welding process. Mater Sci Eng A 435-436:297–304. doi:10.1016/j.msea.2006.07.082
30. Shinoda T, Kondo Y (1997) Friction stir welding of aluminium plate. Weld Int 11:179–184. doi:10.1080/09507119709451948
31. Hwang Y-M, Kang Z-W, Chiou Y-C, Hsu H-H (2008) Experimental study on temperature distributions within the workpiece during friction stir welding of aluminum alloys. Int J Mach Tools Manuf 48:778–787. doi:10.1016/j.ijmachtools.2007.12.003
32. Tang W, Guo X, McCLURE JC et al (1998) Heat input and temperature distribution in friction stir welding. J Mater Process Manuf Sci 7:163–172. doi:10.1106/55TF-PF2G-JBH2-1Q2B
33. Mishra RS, Mahoney MW (2007) Friction stir welding and processing. ASM International, Materials Park, Ohio
34. Chao YJ, Qi X, Tang W (2003) Heat transfer in friction stir welding—experimental and numerical studies. J Manuf Sci Eng 125:138. doi:10.1115/1.1537741
35. Zimmer S, Langlois L, Laye J, Bigot R (2010) Experimental investigation of the influence of the FSW plunge processing parameters on the maximum generated force and torque. Int J Adv Manuf Technol 47:201–215. doi:10.1007/s00170-009-2188-3
36. Atharifar H, Lin D, Kovacevic R (2009) Numerical and experimental investigations on the loads carried by the tool during friction stir welding. J Mater Eng Perform 18:339–350. doi:10.1007/s11665-008-9298-1
37. Su H, Wu CS, Pittner A, Rethmeier M (2013) Simultaneous measurement of tool torque, traverse force and axial force in friction stir welding. J Manuf Process 15:495–500. doi:10.1016/j.jmapro.2013.09.001
38. Frigaard Ø, Grong Ø, Midling OT (2001) A process model for friction stir welding of age hardening aluminum alloys. Metall Mater Trans A 32:1189–1200. doi:10.1007/s11661-001-0128-4
39. Heurtier P, Jones MJ, Desrayaud C et al (2006) Mechanical and thermal modelling of friction stir welding. J Mater Process Technol 171:348–357. doi:10.1016/j.jmatprotec.2005.07.014
40. Sutton M, Yang B, Reynolds A, Taylor R (2002) Microstructural studies of friction stir welds in 2024-T3 aluminum. Mater Sci Eng A 323:160–166. doi:10.1016/S0921-5093(01)01358-2
41. Schneider JA, Nunes AC (2004) Characterization of plastic flow and resulting microtextures in a friction stir weld. Metall Mater Trans B Process Metall Mater Process Sci 35:777–783. doi:10.1007/s11663-004-0018-4
42. Arora A, Nandan R, Reynolds AP, DebRoy T (2009) Torque, power requirement and stir zone geometry in friction stir welding through modeling and experiments. Scr Mater 60:13–16. doi:10.1016/j.scriptamat.2008.08.015